Ga and In adsorption on Si(112): Adsorption sites and superstructure

M. Speckmann, Th. Schmidt,* J. I. Flege, J. Höcker, and J. Falta
Institute of Solid State Physics, University of Bremen, Otto-Hahn-Allee 1, 28 359 Bremen, Germany
(Received 7 September 2016; revised manuscript received 2 March 2017; published 31 March 2017)

The adsorption of the two group-III metals Ga and In on Si(112) has strong influence on the morphology of the intrinsically faceted Si(112) surface. Upon Ga or In adsorption, the Si(112) surface is smoothed, and quasi-1D adsorbate structures along the $[1\bar{1}0]$ direction are observed. These structures consist of $(N\times1)$ building blocks of different sizes, the periodicity of which can be controlled by surface coverage and deposition temperature, as revealed by spot profile analysis low-energy electron diffraction. From x-ray standing-wave measurements, building blocks consisting of two parallel rows of adsorbate atoms are identified for both Ga/Si(112) and In/Si(112). One adsorption site is identified as a terrace (substitutional) site and the other one as a step-edge (adatom) site. These experimental results are compared to several relaxed model structural configurations obtained from density functional theory calculations. In the case of Ga/Si(112), a previously reported structural model by Snijders *et al.* [Phys. Rev. B **72**, 125343 (2005)], including two Ga vacancies per unit cell is corroborated, while for In/Si(112), existing models by Gai *et al.* [Phys. Rev. B **61**, 9928 (2000)] and by Bentmann *et al.* [Phys. Rev. B **80**, 085311 (2009)] can be ruled out, and a new structural model including only one In vacancy per unit cell in the step-edge site is concluded on, similar to the Al/Si(112) model introduced by Gupta and Batra [Phys. Rev. B **72**, 165352 (2005)].

DOI: 10.1103/PhysRevB.95.125441

I. INTRODUCTION

Although not as intensely studied as low-index surfaces like Si(001) or Si(111), high-index surfaces of silicon have attracted significant interest in basic and applied science. They provide a low symmetry combined with a high step density. Both properties can be used, e.g., for the self-assembled growth of anisotropic low-dimensional germanium structures, like nanowires [1–6].

Pre-adsorption of group-III metals on high-index Si surfaces provides an opportunity to strongly influence the morphology and arrangement of subsequently grown Ge nanostructures [7–10]. The adsorption of trivalent metals on Si surfaces may also be used for other applications which require surface passivation. For instance, in hybrid systems, where organic molecules are used for functionalization of semiconductor surfaces, the interaction between the substrate and the organic layer often needs to be reduced to obtain an ordered layer [11–13]. Also in this field of application, the use of high-index Si substrates is promising, as the low symmetry of such substrates can be expected to reduce the number of rotational domains of the layer material.

The clean Si(112) surface is intrinsically unstable and decomposes into (111) and (5 5 12) facets [14,15]. However, it has already been shown [16–21] that the adsorption of group-III elements on Si(112) induces surface smoothening. For Al/Si(112), Ga/Si(112), and In/Si(112), different structural models have been proposed [16–23]. In all these models, the group-III metal atoms adsorb on so-called terrace sites and/or on so-called step-edge sites. Both the step-edge sites as well as the terrace sites are arranged in chains along the $[1\bar{1}0]$ direction. Another common structural element within the different models are vacancies in these chains. These vacancies are a consequence of the large compressive stress imposed on the surface due to the adsorption of group-III metal atoms, similar to the Si(111) surface [24–28]. Baski *et al.* predicted an optimum strain energy compensation for a vacancy distance between five and six unit cells for Ga/Si(112) [29].

Al adsorption leads to a (5×1) reconstruction at coverages well below one monolayer and a transition to a (6×1) reconstruction at around a monolayer [16,21]. Density functional theory (DFT) calculations suggest that Al occupies both the step-edge sites and the terrace sites [22]. Within this model, the chains along the step-edge sites are periodically interrupted by vacancies at every fifth or sixth site, whereas the chains along the terrace sites are continuously occupied with Al.

For Ga on Si(112), a mixture of different $(N\times1)$ reconstructions is found, where (5×1) and (6×1) are the most frequent ones [29]. In earlier studies [16,17,29], a structure with only one adsorption site plus vacancy has been suggested, thus comprising only five Ga atoms per (6×1) unit cell. More recent studies [19,20] with better resolved STM images and additional DFT calculations, however, reveal a structure which is more similar to the Al/Si(112) system. Here, also two adsorption sites (terrace site and step-edge site) are proposed. Contrary to Al/Si(112), both the terrace chain and the step-edge chain are interrupted by one vacancy per (5×1) or (6×1) unit cell. As a result, a so-called vacancy line is formed, perpendicular to the Ga chains. Because the atoms on the step-edge site are shifted by half a (1×1) unit cell in $[1\bar{1}0]$ direction, as compared to the atoms on the terrace sites in the same unit cell, this vacancy line propagates in a zigzag shape along the $[11\bar{1}]$ direction. In this model by Snijders *et al.* [20], each (6×1) unit cell is occupied by 10 Ga atoms.

The situation for In adsorption on the Si(112) surface, however, is contentious. In a publication by Gai *et al.* [18], a (4×1) reconstruction is found at a growth temperature of 400 °C and a coverage of around $\frac{2}{3}$ ML, which is reported to merge into a (7×1) reconstruction after annealing at 450 °C with a saturation coverage of around $\frac{1}{3}$ ML. In the (7×1) unit cell a single vacancy is suggested, similar to Ga or Al

*Corresponding author: tschmidt@ifp.uni-bremen.de

adsorption, but in this structure the indium atoms are stated to occupy *terrace sites only*. Later, a theoretical study by Bentmann *et al.* confirmed the stability of a (7×1) unit cell, but they proposed the occupation of *step-edge sites only* [23].

In the present paper, we provide a comprehensive structural analysis of the Ga and In passivated Si(112) surface, which has been accomplished by using a variety of experimental and theoretical tools. With spot profile analysis low-energy electron diffraction (SPA-LEED) and with scanning tunneling microscopy (STM), the average and the local periodicity of the surface have been investigated in dependence of coverage and adsorption temperature. From these results, the existence of $(N\times1)$ building blocks with vacancies is identified for both Ga and In adsorption. In the next step, the internal atomic structure of the building blocks is revealed by combining x-ray standing waves (XSW) experiments with DFT calculations. This combination has already been successfully applied to a variety of adsorbate systems on silicon surfaces [25,30–33]. In the present case, this approach confirms the model by Snijders *et al.* for Ga/Si(112), whereas the only available models for In/Si(112), which imply a 7×1 reconstruction [18,23], can be ruled out, and a different model is suggested instead.

We will show that Ga/Si(112), In/Si(112), and, in regard of literature [22], also Al/Si(112) share several structural elements which therefore can be assigned to be universal for adsorption of group-III metals on Si(112). As will be shown, these metal adatoms are arranged in one-dimensional chains which are accompanied by vacancies, the latter inducing a geometric distortion along the chains. This is manifested in the formation of mixed pentamers or hexamers. Though we focus on structural properties in this paper, we note that these modulated one-dimensional structures may exhibit interesting electronic properties, like charge-density waves, similar to In/Si(111)-(4×1) [34,35].

II. EXPERIMENTAL AND COMPUTATIONAL DETAILS

The first part of the experiments discussed in the following was carried out under ultrahigh vacuum (UHV) conditions in the scanning tunneling microscopy (STM) and spot-profile analysis low-energy electron diffraction (SPA-LEED) [36,37] laboratories of our institute. The STM setup is additionally equipped with a conventional LEED instrument. Some of the LEED patterns shown in the following were recorded using the Elmitec III low-energy electron microscopy at beamline U5UA of the National Synchrotron Light Source (NSLS) at Brookhaven National Laboratory (BNL) [38].

The x-ray standing-waves experiments, which are presented in the second part, were performed *in situ*, employing the UHV setup at the undulator beamline BW1 at the Hamburg synchrotron radiation laboratory (HASYLAB). A standard, nondispersive monochromator setup using pairs of symmetrically and asymmetrically cut crystals was used for XSW measurements in (111) and (113) Bragg reflection geometries. Additionally, XSW experiments were performed dispersively in (202) and (022) Bragg reflection geometries with a Si(111) monochromator setup. For the XSW measurements, the incident photon energy was tuned through a Bragg condition. Simultaneously, either photoemission or fluorescence spectra were recorded with a CLAM 100 electron energy analyzer or with a Si(Li) fluorescence detector, respectively. From these spectra, the net Si $1s$, Ga $2p_{3/2}$, or In $2p_{3/2}$ photoemission yields, or the net Si K and In L fluorescence yields, respectively, were determined and analyzed according to the dynamical theory of x-ray diffraction [39,40].

Based on the XSW results, as will be detailed later, different structural models have been compiled and refined using *ab-initio* DFT within the local-density approximation, employing a plane-wave basis set as implemented in the program package PWscf [41,42]. Self-consistent solutions to the Kohn-Sham equations were obtained using a converged (2×3×1) $\vec{k}$ point grid in the surface Brillouin zone. An electronic high-energy cutoff of 20 Ry was found to be sufficient in order to ensure convergence not only with respect to the total energy, but also regarding the resulting geometric structure and, more specifically, its Fourier components in the XSW simulation, which poses an additional criterion in the quantitative XSW analysis of DFT-calculated structures [32].

The electron-ion interaction has been considered in the form of *ab initio* norm-conserving pseudopotentials [43,44]. In the repeated-slab models of the (3×1), (4×1), (5×1), and (6×1) supercells, 6 Si bilayers have been implemented to account for the relaxation of the upper-most surface layers. During the relaxation, the lowest two Si layers have been fixed to ideal bulk coordinates. For the analysis of the DFT results, these layers also serve as a reference in the XSW simulation of the structural models, i.e., the calculation of the (111), (113), (202), and (022) Fourier components of the adsorbate atoms within the relaxed model configurations. The corresponding lattice plane spacings are $d_{(111)} = a_0/\sqrt{3} = 3.136$ Å, $d_{(113)} = a_0/\sqrt{11} = 1.638$ Å, and $d_{\{202\}} = a_0/\sqrt{8} = 1.920$ Å, respectively, where $a_0 = 5.431$ Å is the cubic lattice constant of Si.

The Si(112) substrates were cut from commercially available Si wafers with a miscut of less than 0.1°. After cleaning with methanol or ethanol, they were introduced into the vacuum systems and degassed at about 600 °C for at least 12 hours. The sample heating was accomplished by direct current heating. The temperature was monitored using an infrared pyrometer. The STM images were recorded and analyzed with the program GXSM by Zahl *et al.* [45,46].

The faceted Si(112) starting surface [14,15,47] was prepared by flash heating up to about 1250 °C. Either Ga or In was deposited on the clean Si(112) surface, until a saturation coverage was reached and the LEED pattern did not change anymore. For the Ga and In deposition, temperatures ranging from 500 to 660 °C and from 390 to 520 °C were chosen, respectively. Both materials were evaporated from e-beam evaporators. After Ga or In deposition, the samples were cooled down to room temperature immediately in order to prevent Ga or In redesorption. All preparation steps were monitored by LEED or SPA-LEED.

The evaporator fluxes were calibrated in separate experiments on Si(111) from the well-known $(\sqrt{3}\times\sqrt{3})$-R 30°-In and (4×1)-In reconstructions and the $(\sqrt{3}\times\sqrt{3})$-R 30°-Ga and (6.3×6.3)-Ga reconstructions, respectively. The $(\sqrt{3}\times\sqrt{3})$-R 30°-Ga structure is completely developed [25,30,48] at a Ga coverage of exactly $\frac{1}{3}$ ML_{111}, where 1 ML_{111} corresponds to 7.83×10^{14} atoms/cm^2. The $(\sqrt{3}\times\sqrt{3})$-R 30°-In

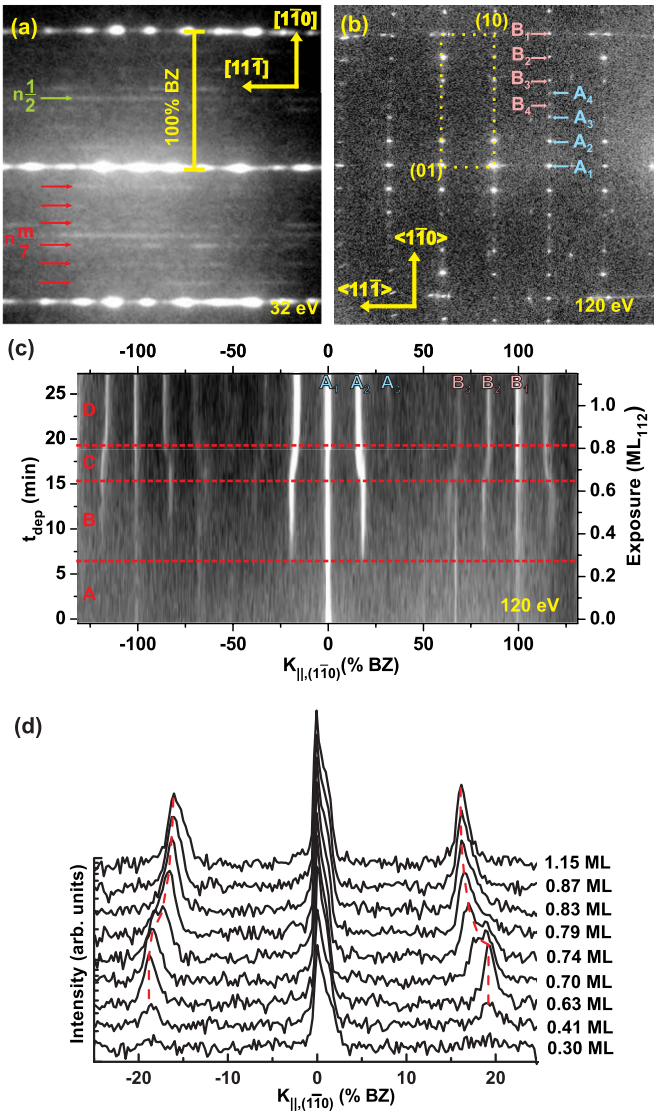

FIG. 1. Coverage dependence of the Ga/Si(112) surface. LEED patterns of (a) clean Si(112) and (b) after Ga saturation of the Si(112) surface at 660 °C. Line scans through (00) along the [1$\bar{1}$0] direction recorded during Ga deposition on clean Si(112) at 540 °C are shown in frames (c) and (d).

reconstruction is completely evolved [49–51] at a coverage of $\frac{1}{3}$ ML_{111} and the (4×1) reconstruction at a coverage of 1 ML_{111} [50,52,53]. For this publication (if not indicated differently) 1 ML refers to 1 ML_{112}, which equals 5.54 × 10^{14} cm^{-2}.

III. RESULTS AND DISCUSSION

A. Reconstruction of the Ga/Si(112) surface

A typical LEED pattern of the clean Si(112) surface with (111) and (5 5 12) facets is shown in Fig. 1(a). All spots line up in rows along the [11$\bar{1}$] direction. Additionally to the integer order stripes, spots occur at $\frac{n}{7}$ and $\frac{1}{2}$ of the surface Brillouin zone (BZ), as indicated with the red and green arrows, respectively. These spots can be assigned to (7×7) reconstructed (111) facets and to (5 5 12) facets with a (2×1) reconstruction [15,54].

Upon Ga adsorption, the surface is smoothed and the structure changes to an ($\overline{N}$×1) reconstruction. (Here and in the following, we denote the average periodicity of the surface with $\overline{N}$, which can take noninteger values, while the integer N refers to the size, in units of the 1×1 unit mesh size, of an underlying building block, as used for model calculations in Sec. III C.) A corresponding LEED pattern is shown in Fig. 1(b). A reciprocal (1×1) unit mesh is marked with a dotted yellow rectangle. The superstructure spots labeled A_1 to A_4 and the spots denoted by B_1 to B_4 have the same distance to each other, respectively. The distance for this sample is roughly 18% BZ and, thus, a periodicity of $\overline{N} \approx 5.5$ is obtained after Ga deposition at around 660 °C. To have a closer look at the evolution of this reconstruction, we recorded a so-called time plot, which is given in Fig. 1(c) for a deposition temperature of 540 °C. Here, we took line scans along the [1$\bar{1}$0] direction through the center of the first Brillouin zone (BZ). An electron energy of 120 eV was chosen, where two facets spots overlap each other in the center of the BZ and form a 'pseudo (00) spot,' which makes sample alignment easier.

At the beginning of the deposition (stage 'A') no evidence for a change of the superstructure is visible, as the diffraction line profile remains unchanged. At a Ga exposure of roughly 0.3 ML additional superstructure spots appear at ±19% BZ and at ±81% BZ, which is equivalent to a periodicity of $\overline{N} = 5.26 \pm 0.05$. The last remnants of the faceted structure vanish at around 0.5 ML. In this stage of the deposition (stage 'B') the intensity of the new superstructure spots increases, indicating that the ($\overline{N}$×1) structure covers an increasing fraction of the surface. The position of these superstructure spots, however, remains constant up to a Ga exposure of around 0.65 ML. When this coverage is reached, the superstructure spots change their position in [1$\bar{1}$0] direction quite rapidly (stage 'C'). Additionally, all other spots appear that belong to the ($\overline{N}$×1) reconstruction. All superstructure spots move towards the integer order spots, as can be seen from Fig. 1(d) in more detail. Thus, the real-space period length of the superstructure is increased in this stage. At an exposure of around 0.8 ML, which is around the value of the saturation coverage of this structure [55], the final stage 'D' is reached. For the chosen deposition conditions, the first order superstructure spots end up at around ±16% BZ, corresponding to a periodicity of $\overline{N} = 6.25 \pm 0.05$.

The local structure of the ($\overline{N}$×1) surface is depicted in Fig. 2(a), where a typical STM image after Ga deposition at 550 °C is given. In agreement with the LEED results discussed above, the surface is atomically flat, i.e., no facets are found. In Fig. 2(a), two terraces can be identified, separated by a step edge that runs from the top to the bottom of the image. Already in this larger-scale view one can realize unit cells of different sizes that are interrupted by vacancies (dark stripes along [11$\bar{1}$]). This can be seen more clearly from Fig. 2(b), where a zoom into the region marked with a yellow box in (a) is shown. Here, several (6×1) and (5×1) unit cells can be identified. These unit cells comprise two stripes along the [1$\bar{1}$0] direction, a broader bright one and a thinner dark one. Additionally, in every unit cell vacancies can be found (indicated by white dots) that form vacancy lines along the [1$\bar{1}$0] direction. These

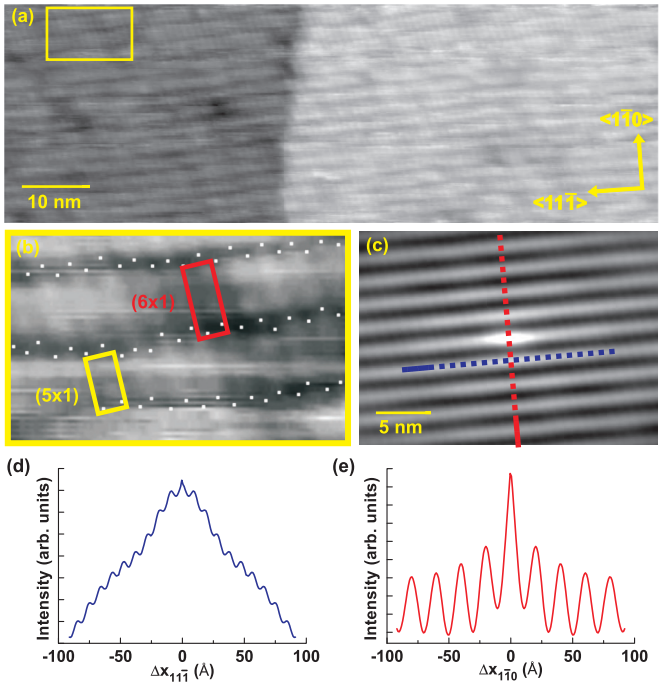

FIG. 2. (a) Filled-state STM image (tip bias = +2.0 V, $I = 1.0$ nA) of 0.3 ML Ga/Si(112) deposited at 550 °C. (b) Zoom into the area marked with the yellow box in frame (a). (c) Autocorrelation of the STM image shown in frame (a). The cross-sections along (d) [11$\bar{1}$] and (e) [1$\bar{1}$0] were taken along the lines indicated in frame (c).

vacancy lines extend over the whole surface and are only interrupted by step edges or defects. However, they are not perfectly straight but have a zigzag arrangement on atomic scale and a meandering appearance on larger scale.

Whereas the meandering of the vacancy lines is a direct consequence of the coexistence of different unit cell sizes, as reported in earlier publications [19,20], the zigzag arrangement points to the presence of two different adsorption site chains that are interrupted by neighboring vacancies. This interpretation is further supported by the above-mentioned finding of a dark and a bright stripe in each unit cell, since a very similar stripe pattern in filled-state images has been predicted in DFT based STM simulations for the two-site chain model proposed by Snijders *et al.* [20]. Although the atomic structure within the unit cells can hardly be determined using STM alone, our data corroborates that model, with eight Ga atoms in one (5×1) unit mesh (four at both the step-edge sites and the terrace sites, plus two vacancies), or, accordingly, with 10 Ga atoms in one (6×1) unit mesh. Hence, this model implies a saturation coverage of 8/10 ML or 10/12 ML for a completely (5×1) or completely (6×1) reconstructed surface, respectively. With this knowledge also the results shown in Fig. 1 can be explained: At the beginning of stage 'C' the surface consists of more (5×1) than (6×1) building blocks. As the coverage increases, the number of (6×1) building blocks is increasing, which results in an increased average period length. When the saturation coverage is reached, no change in this periodicity is found anymore, and the final stage 'D' is obtained. Hence, the noninteger periodicity as observed in the LEED patterns is attributed to a mixture of (N×1) building blocks rather than to a truly incommensurate reconstruction.

For a complementary determination of the surface periodicity by STM, we calculated the autocorrelation function of the image data shown in Fig. 2(a). The autocorrelation function is a convolution of the measured signal (after subtracting its mean value) with itself. The result is shown in Fig. 2(c). Since the strongest contrast in the STM image is generated by the quite regularly arranged vacancy lines along the [11$\bar{1}$] direction, also the autocorrelation data shows a pronounced stripe pattern along that direction. Within these stripes, i.e., in the [11$\bar{1}$] direction, a weaker modulation contrast appears in Fig. 2(c), which can be attributed to the spatial correlation of the adsorbate chains. The period length along the [11$\bar{1}$] and [1$\bar{1}$0] directions have been analyzed separately by taking line profiles along these directions, which are shown in Figs. 2(d) and 2(e), respectively. Along the [11$\bar{1}$] direction [cf. Fig. 2(d)], correlation maxima are found at integer multiples of (9.8 ± 0.2) Å, which is in reasonable accordance with the unit cell size of 9.41 Å of the bulk truncated Si(112) surface. The discrepancy of about 4% can be assigned to inaccuracies of the STM calibration and, e.g., thermal drift. From Fig. 2(e), a period length of (20.7 ± 0.4) Å is determined along the [1$\bar{1}$0] direction, which corresponds to (5.39 ± 0.10) times the bulk truncated unit cell size in that direction. This value is in good agreement with the value of $\overline{N} = 5.26 \pm 0.05$ that has been determined by SPA-LEED for similar deposition temperature and coverage, as mentioned above.

To address the temperature dependence of the reconstruction of the Ga/Si(112) surface, we deposited Ga at different temperatures, until saturation coverage was reached, and subsequently determined the periodicity of the reconstruction by means of SPA-LEED. Two exemplary diffraction patterns that have been recorded at room temperature after deposition of Ga at 620 °C and 660 °C are shown in Figs. 3(a) and 3(b), respectively. For the former sample the average reconstruction is exactly (6×1), whereas for the latter one the superstructure spots have a larger distance to each other, corresponding to a reduction of the average period length in real space.

The change of the diffraction pattern can be seen in more detail in the viewgraph in Fig. 3(c), where line scans along the [1$\bar{1}$0] direction through the (00) spot are shown for different deposition temperatures. With increasing deposition temperature the superstructure spots move away from the (00) spot, indicating a smaller period length at higher deposition temperatures. Within the temperature range from 500 °C to 660 °C investigated here, the periodicity decreases from $\overline{N} = 6.50 \pm 0.05$ to 5.53 ± 0.05, as shown in Fig. 3(d). For even higher temperatures, the Ga termination of the Si(112) surfaces becomes unstable and facets appear again. Already for 660 °C, weak diffraction spots, which we assign to facets, can be seen in Fig. 3(c) at $K_{\parallel} \approx \pm 6\%$ BZ. This indicates that a small fraction of the surface is already free of Ga, which implies a significant desorption rate at this temperature.

From our results it is obvious that only at deposition temperatures above 620 °C an agreement with previously reported energy minimization calculations [29,56] is reached. In these publications a minimum of the surface free energy of the (N × 1) reconstruction is found at a value of N in the range from 5 to 6. However, at lower deposition temperatures we find that the periodicity is well above $N = 6$, and thus a

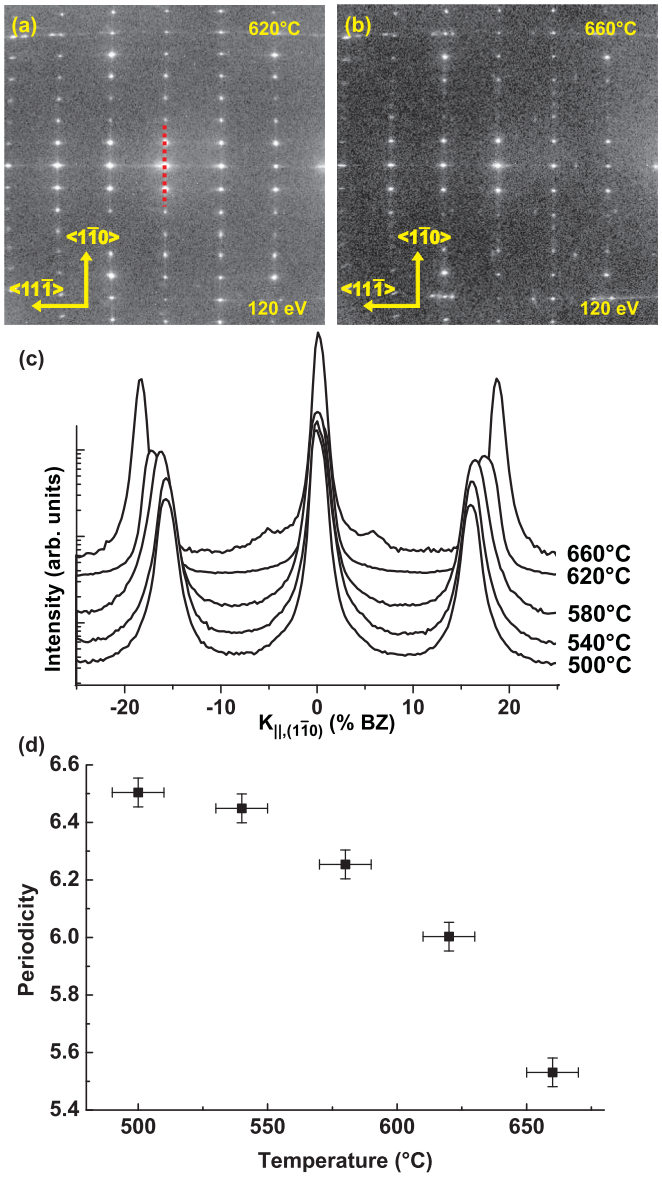

FIG. 3. Temperature dependence of the Ga/Si(112) surface. SPA-LEED patterns of Si(112) after Ga deposition at (a) 620 °C and (b) 660 °C. (c) Line scans along the dotted line in (a) for different deposition temperatures. (d) Periodicity of the superstructure as function of the deposition temperature.

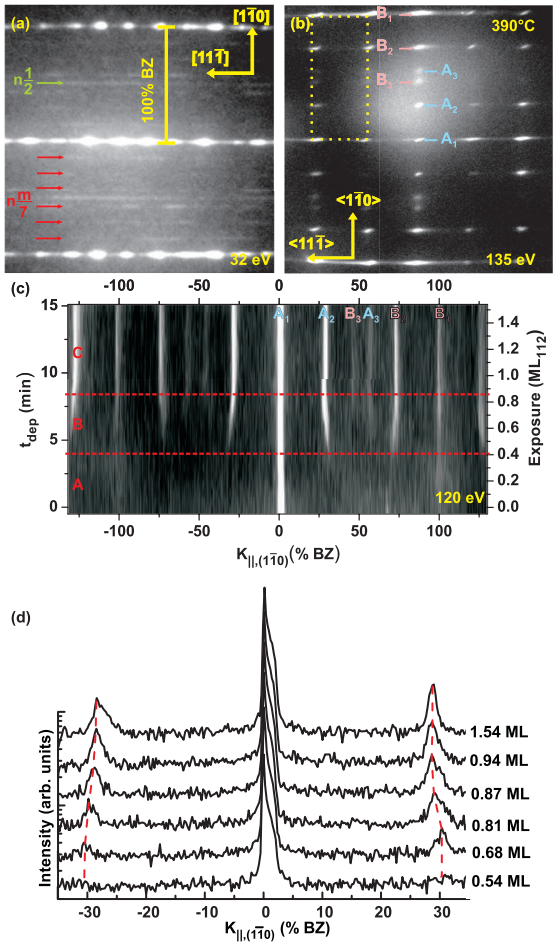

FIG. 4. Coverage dependence of the In/Si(112) surface. LEED patterns of (a) clean Si(112) and (b) after In saturation of the Si(112) surface at 390 °C. Line scans through (00) along the [1$\bar{1}$0] direction recorded during In deposition on clean Si(112) at 450 °C are shown in frames (c) and (d).

significant fraction of (7×1) or even (8×1) unit cells must be present on the surface.

The data presented so far suggest that the average periodicity $\overline{N}$ depends both on the coverage and on the deposition temperature. By recalling, however, that the Ga/Si(112) surface consists of $(N\times1)$ building blocks with vacancies, combined with straightforward considerations, these dependencies can be brought together, as follows. With increasing coverage at constant temperature, we find that $\overline{N}$ increases. This provides further support for the Ga vacancy model of the $(N\times1)$ building blocks, since an increase of coverage will imply a reduced density of vacancies which can be achieved by an increase of the average building block size $\overline{N}$. With increasing temperature, we find that the value for $\overline{N}$ at saturation coverage decreases. In other words: an increase in temperature has the same effect as a reduction of the coverage. This is easily understood since with increasing temperature the sticking coefficient will be reduced, and the desorption rate is increased, as evidenced above. Hence, for a fixed Ga deposition rate, the saturation coverage can be expected to be diminished at higher temperatures, which is obviously accomplished by a higher density of vacancy lines, leading to the observed decrease of $\overline{N}$. The value of $\overline{N}$ can be interpreted as an optimum compromise between Ga-Si adsorption energy on the one hand (which disfavors vacancies), and strain energy on the other hand (which favors a large density of vacancies). Depending on whether the boundary conditions are Ga rich or Ga poor, the balance between these competing interactions can be shifted.

B. Reconstruction of the In/Si(112) surface

The adsorption of In on Si(112) has very similar characteristics as compared to Ga/Si(112). The change of the LEED pattern as induced by In saturation is illustrated in Figs. 4(a) and 4(b). The Si(112) surface is smoothed upon In adsorption and an $(\overline{N}\times1)$ reconstruction is obtained. One (1×1) unit cell

is marked with a dotted yellow rectangle in Fig. 4(b). The spots labeled A_1 to A_3 and the spots marked with B_1 to B_3 have the same distance to each other, respectively. The distance for this sample is roughly 27% BZ and, thus, a periodicity of $\overline{N} \approx 3.7$ is obtained after In deposition at around 390 °C. However, the In/Si(112) surface is not completely de-faceted, as can be seen from the streaky integer order spots in Fig. 4(b).

The evolution of the reconstruction during In adsorption at 450 °C is shown in the time plot in Fig. 4(c). The plot looks very similar to the plot in Fig. 1(c), but there are noteworthy differences. The first stage 'A,' where no In-induced superstructure spots are visible, persists longer, up to an In exposure of about 0.4 ML. In the second stage 'B,' the superstructure spots evolve. As soon as they appear, they start to move towards the integer order spots. This is different as compared to Ga/Si(112), where the positions of the superstructure spots remain constant for an extended deposit range and start to move at a later stage. The final stage 'C,' in which the superstructure spots have reached their final positions, is achieved after the adsorption of roughly 0.85 ML. This is a similar value as for Ga/Si(112) (cf. Sec. III A) and is in good agreement with previously reported results for the saturation coverage [10]. For the chosen deposition temperature the first-order superstructure spots end up at ±28% BZ, which is equivalent to a periodicity of $\overline{N} \approx 3.5$. The change of the superstructure spots with increasing coverage can also be seen from Fig. 4(d), where line scans at different In exposures are shown.

The final periodicity of $\overline{N} \approx 3.5$ observed here could, in principle, also be explained by a (7×1) reconstruction as proposed by Gai *et al.* [18] and by Bentmann *et al.* [23]. These authors suggest that the surface consists of (7×1) unit cells. If vanishing form factors are assumed for diffraction spots like $(n\frac{1}{7})$ and $(n\frac{6}{7})$, the LEED pattern of a (7×1) reconstructed surface is very similar to that of an $(\overline{N}\times 1)$ surface with $\overline{N} \approx 3.5$. From our data recorded during In adsorption, however, it is evident that the surface reconstruction consists of (3×1) and (4×1) building blocks with variable abundance, because otherwise the shift of the superstructure spots could not be explained. Moreover, for $\overline{N} = 3.5$, the presence of (4×1) and (3×1) building blocks *without* long-range alternating ordering easily explains the "missing" seventh-order spots, without any requirements on the form factors. This has recently been pointed out in a LEED study on ceria films on Ru(0001) [57].

The scheme of co-existing (3×1) and (4×1) building blocks is further supported by measurements in dependence of the deposition temperature, which are shown in Fig. 5. From the two depicted LEED patterns in Figs. 5(a) and 5(b) and the associated line scans in Fig. 5(c) a shift of the superstructure spots away from the integer order spots is obvious for increasing deposition temperature. Hence, at higher temperatures a smaller value of the periodicity $\overline{N}$ is present on the In-covered Si(112) surface. The periodicity as a function of the deposition temperature is shown in more detail in Fig. 5(d). Within the investigated temperature range from 390 °C to 520 °C, $\overline{N}$ decreases from about 3.70 to about 3.48.

Combining the experimental results presented in Figs. 4 and 5, and with the same reasoning as for Ga/Si(112)-$(\overline{N}\times 1)$ in the previous section, we conclude that the periodicity of the In/Si(112)-$(\overline{N}\times 1)$ surface is mainly governed by the In

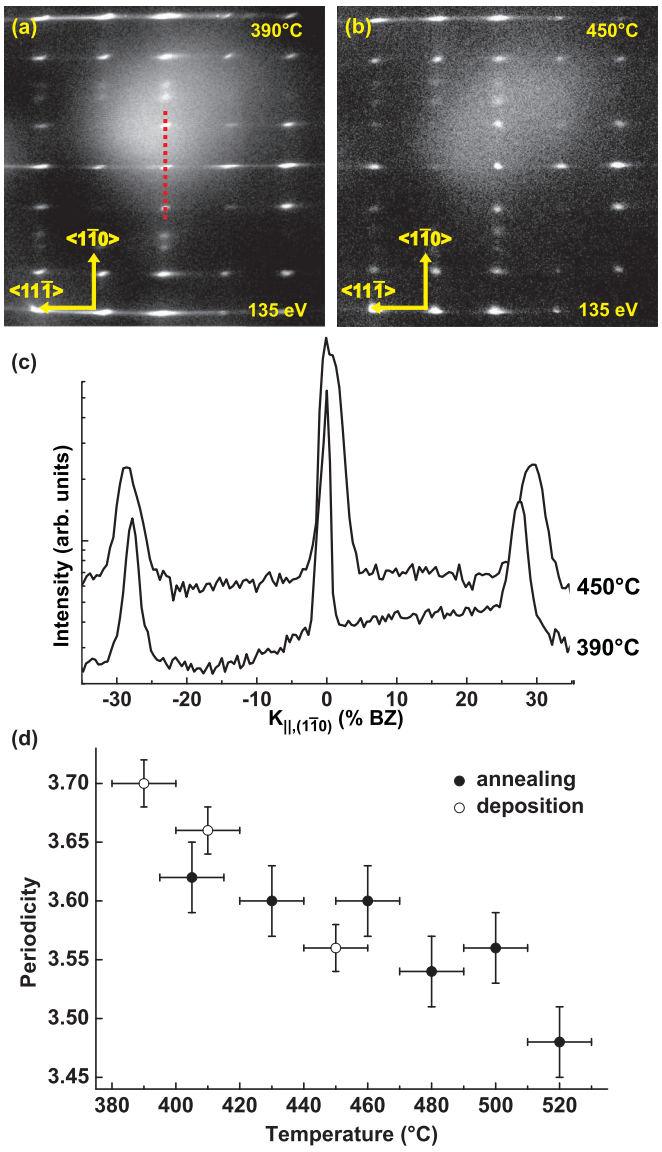

FIG. 5. Temperature dependence of the In/Si(112) surface. SPA-LEED patterns of Si(112) after In deposition at (a) 390 °C and (b) 450 °C. (c) Line scans along the dotted line in (a) for different deposition temperatures. (d) Periodicity of the superstructure as function of the deposition/annealing temperature. The filled circles correspond to In saturation at 390 °C and repeated annealing for 3 minutes at increasing temperatures.

coverage. The saturation coverage at fixed In deposition rate can be expected to be lowered at higher temperatures. As a consequence, a larger density of In vacancies, corresponding to a smaller value of $\overline{N}$, is not only observed in the initial stages of In adsorption but, equivalently, also for In saturation at high temperatures. Hence, our results strongly support vacancies as structural elements for the In/Si(112)-$(\overline{N}\times 1)$ system.

Vacancies have also been proposed by Gai *et al.* [18] and by Bentmann *et al.* [23]. However, In atoms are supposed to occupy only one type of adsorption sites in these models, which implies a saturation coverage of less than 0.5 ML. In contrast, our SPA-LEED data indicate a significantly higher

saturation coverage of about 0.85 ML. This value indicates that the In-induced structure is more similar to the Ga- or Al-induced structures on Si(112), i.e., with two adsorption sites, as will be evidenced more clearly by XSW and DFT below. The relatively high saturation coverage in spite of the low period length suggests that, opposed to the Ga/Si(112) structure [20] but in accordance with Al/Si(112)[22], only a vacancy in one of the two adsorption site chains is present. Hence, one (3×1) unit cell would contain five In atoms (three on one adsorption site chain and two on the other chain, plus one vacancy) and a (4×1) unit cell would contain seven In atoms, resulting in a saturation coverage of 5/6 or 7/8 ML, respectively. The experimentally observed value for a surface with a mixture of (3×1) and (4×1) building blocks is in the range between these two values (≈ 0.85 ML, cf. Fig. 4). If, however, two vacancies per building block are assumed (one in each adsorption site chain), a saturation coverage between 4/6 ML and 6/8 ML is expected. In regard of the data presented in Fig. 4 and an estimated inaccuracy of the coverage determination of 10%, the latter model cannot be clearly ruled out, but seems unlikely.

C. Atomic structure of Ga- and In-induced reconstructions

From the STM and SPA-LEED results discussed in the previous sections, it is clear that both the Ga/Si(112) and the In/Si(112) surface consists of $(N\times1)$ building blocks. In order to investigate the internal structure of these building blocks and, hence, to be able to establish a structural model for both the Ga/Si(112) and the In/Si(112) structures, we performed x-ray standing-wave (XSW) measurements and, complementary, density functional theory (DFT) calculations.

XSW allows us to directly determine the position of adsorbate atoms at the surface relative to the crystal lattice with picometer resolution [58]. By the coherent superposition of incoming and Bragg-reflected x rays a standing-wave field, which is temporally and spatially coherent, is generated. The nodal and antinodal planes of the standing-wave field are parallel to the diffraction planes and have the same periodicity. If the reflectivity and a secondary signal (i.e., an inelastic, element-specific signal, in our case fluorescence or photoemission) is recorded, information about the spatial distribution of the elements on the surface can be obtained. The intensity of the secondary signal is given [58] by the so-called yield function Y, which is the sum over the individual yields Y_i from atoms located at $\vec{r}_i$ that experience the local standing-wave field's intensity $I(\vec{r})$:

$$\begin{aligned} Y &= \sum_i Y_i \propto \sum_i I(\vec{r}_i) \\ &\propto 1 + R + 2\sqrt{R}\, f_c \cos(\nu - 2\pi\Phi_c) =: Y_N, \end{aligned} \tag{1}$$

with the reflectivity R of the sample and the phase ν between incoming and reflected wave. For XSW experiments only the normalized yield Y_N is relevant. It contains two key parameters, the coherent fraction f_c and the coherent position Φ_c, which are the modulus and the phase, respectively, of the $\vec{H}^{\text{th}}$ Fourier component A_H of the atomic distribution function,

$$A_H = \frac{1}{N}\sum_{n=1}^{N} e^{2\pi i \vec{H}\cdot\vec{r}_n} = f_c \cdot e^{2\pi i \Phi_c}, \tag{2}$$

where $\vec{H}$ is the reciprocal lattice vector associated with the Bragg reflection and N the number of atoms contributing to the secondary signal. For a simple system with only one possible adsorption site these two parameters can be interpreted as follows: The coherent position Φ_c is the position of the atoms relative to the diffraction planes in units of the diffraction plane spacing, i.e., $\Phi_c = 1$ (or, equivalently, $\Phi_c = 0$) means that the atoms are on the planes and $\Phi_c = 0.5$ means that the atoms are in the middle between two planes. For such a single-adsorption-site system, and if static disorder and thermal vibrations are neglected, the coherent fraction f_c equals unity. For systems with two or more inequivalent positions, the value of f_c is lowered.

In the case of two different adsorption sites, which will become relevant in the following, Eq. (2) can be rewritten as

$$f_c \cdot e^{2\pi i \Phi_c} = \frac{1}{2}(e^{2\pi i \Phi_1} + e^{2\pi i \Phi_2}), \tag{3}$$

where Φ_1 and Φ_2 are the two possible sites for the adsorbate. This directly leads to

$$\Phi_c = \tfrac{1}{2}(\Phi_1 + \Phi_2) \quad \text{and} \tag{4}$$

$$f_c = \cos(\pi(\Phi_1 - \Phi_2)). \tag{5}$$

Hence, the two positions Φ_1 and Φ_2 can be obtained from the experimentally determinable magnitudes f_c and Φ_c via

$$\Phi_{1,2} = \Phi_c \pm \Delta\Phi \quad \text{and} \tag{6}$$

$$\Delta\Phi = \frac{\arccos(f_c)}{2\pi}. \tag{7}$$

The XSW results for Ga/Si(112) and In/Si(112) are shown in Figs. 6 and 7, respectively. From the Si 1s photoelectron yields and the Si K fluorescence yield, which have been recorded for reference, coherent positions of approximately 1.0 are obtained, as expected for the substrate. The corresponding coherent fractions for Si are close to the expected value of 1.0 for the (202) and (022) Bragg reflections, whereas the (111) and (113) coherent fractions for Si are close to $\sqrt{1/2}$ which is the expected value for these reflections in the diamond structure. The small deviations of the Si coherent fractions and positions from their expected values can be attributed to (i) experimental uncertainties, (ii) thermal vibrations which, via the Debye-Waller factor, will lead to a slightly diminished coherent fraction, and (iii) the fact that nondipole contributions in the photoelectron yields have not been taken into account in our data evaluation. The latter approximation can lead to small shifts of the coherent positions as well as slight increases or decreases of the coherent fractions [59,60]. Opposed to the silicon substrate, disorder might be significant for the adsorbate species. For instance, surplus Ga and In tend to form metallic droplets on the surface that do not have a coherent relationship to the substrate lattice and will reduce the observed

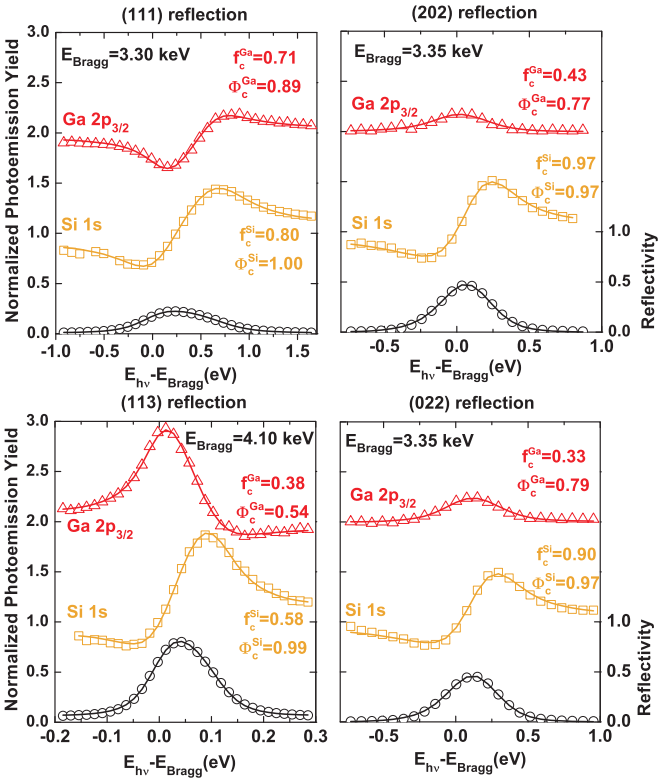

FIG. 6. XSW data (symbols) and fits (solid lines) for Ga/Si(112)-($\overline{N}\times1$). The reflectivities (○) and photoelectron yields for Ga (△) and Si (□) are shown for (111), (113), (202), and (022) Bragg reflections. For better visibility, the Ga yield is shifted by +1.

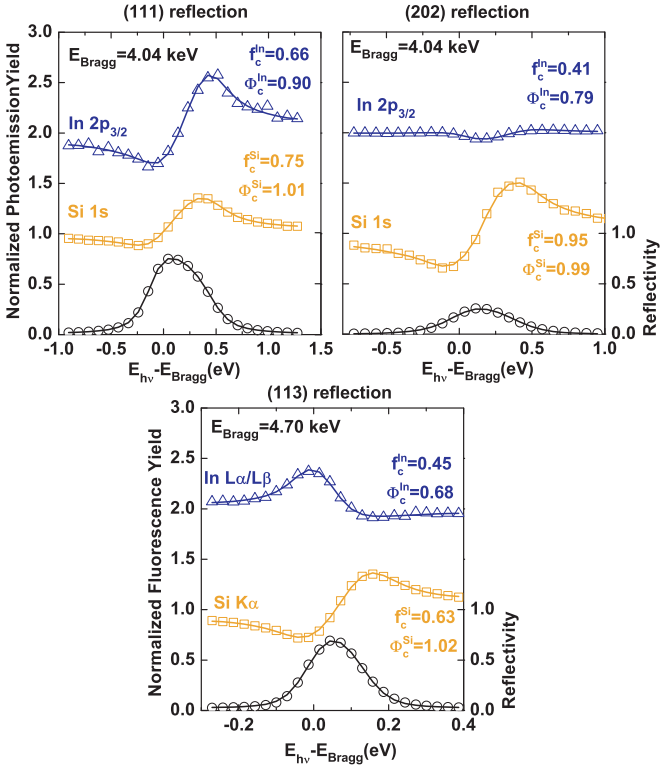

FIG. 7. XSW data (symbols) and fits (solid lines) for In/Si(112)-($\overline{N}\times1$). The reflectivities (○) and photoelectron or fluorescence yields for In (△) and Si (□) are shown for (111), (113), and (202) Bragg reflections. For better visibility, the In yield is shifted by +1.

coherent fractions. This has to be kept in mind when comparing the experimental results with model structures later on.

When comparing Figs. 6 and 7 to each other, it becomes obvious that the results for Ga and In are strikingly similar. For all Bragg reflections investigated here, the coherent positions and fractions for In differ from those for Ga by only a few percent. This is a clear indication that both adsorbate structures are very similar to each other.

From the XSW results, a single-site adsorption geometry can clearly be ruled out for both Ga/Si(112) and In/Si(112). According to Eq. (2), single-site adsorption would imply coherent fractions close to unity for all Bragg reflections. For both adsorbates, however, significantly lower coherent fractions are found, which cannot solely be explained by thermal vibrations and nondipole photoemission contributions. Also random disorder, e.g., by droplet formation, fails as an explanation, since this should affect the coherent fractions for all Bragg reflections equally. This is in contrast to the experimental finding that the values of f_c for (111) Bragg reflection geometry are significantly larger than those for the (113) and (202) reflections. Hence, at least two different adsorption sites have to be occupied on both surfaces.

As mentioned above, from each XSW data set one Fourier component of the spatial distribution function of the adsorbate atoms is determined. In the present case, the number of non-collinear Fourier components (up to four) is rather high from an experimental point of view. However, from literature [16–23] and from the results presented in Secs. III A and III B, up to $2N-1$ adsorption sites have to be taken into account for an ($N\times1$) unit cell, e.g., up to eleven atoms for a (6×1) cell. Hence, it is still impossible to directly conclude on the atomic position of each adsorbate atom within the unit cell from our data. (This is additionally impeded by the fact that different unit cell sizes coexist.) Nevertheless, the results presented so far suggest that Ga and In occupy two chains of adsorption sites that extend along the $[1\bar{1}0]$ direction. Therefore, the XSW results for (111) and (113) reflections can be used to determine the average position of these two adsorbate chains in the $(1\bar{1}0)$ plane. According to Eq. (2) this is possible, because the (111) and (113) reciprocal lattice vectors are perpendicular to the $[1\bar{1}0]$ direction, and thus, only the atomic coordinates within the $(1\bar{1}0)$ plane are probed in (111) and (113) experiments.

Assuming that, in a first approximation, both atomic chains are populated equally, the simple two-position model described above can be used. Applying Eq. (6) to the XSW results in (111) and (113) reflections as presented in Figs. 6 and 7, the positions shown in Table I are determined. In the next

TABLE I. Coherent positions Φ_1 and Φ_2 in a simple two-position model for Ga/Si(112) and In/Si(112) in (111) and (113) Bragg reflections.

adsorbate	Φ_1^{111}	Φ_2^{111}	Φ_1^{113}	Φ_2^{113}
Ga	1.014	0.766	0.726	0.354
In	1.036	0.765	0.716	0.365

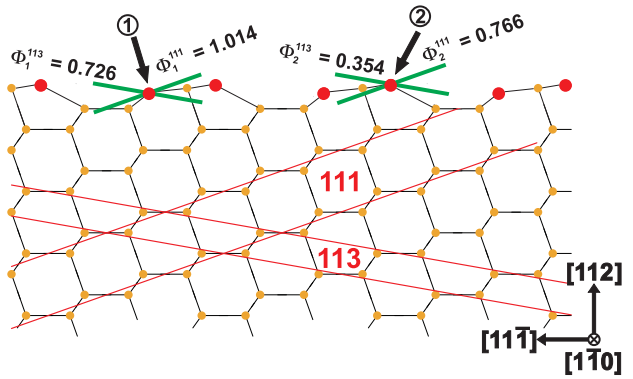

FIG. 8. Two-position model in two dimensions for Ga/Si(112) using the XSW results in (111) and (113) Bragg reflection as listed in Table I. Position '1' corresponds to substitutional (terrace) sites and position '2' to adatom (step-edge) sites.

step, these values can be used to locate each of the adsorption chains in the (1$\bar{1}$0) plane. The result is shown for Ga/Si(112) in Fig. 8. [The corresponding drawing for In/Si(112) looks virtually the same and is, therefore, not shown.] The sites along the chain labeled '1' in Fig. 8 can be identified as substitutional adsorption sites, whereas on the chain labeled '2,' the atoms reside on step-edge sites. Compared to bulk Si atomic positions, the substitutional sites '1' are somewhat inwardly relaxed. This is in agreement with, e.g., Ga/Si(111)-(6.3×6.3), where also an inward relaxation was observed and attributed to the preferential sp^2 hybridization of the trivalent metal, which favors a rather planar bonding geometry [27,61]. From Fig. 8, a similarly planar geometry is also found for the step-edge sites.

Whether the Ga and In bonding geometries are rather planar or not also depends on the position of the neighboring Si atoms. In the drawing in Fig. 8, which is solely based on XSW results, Si bulk positions have been assumed, since no

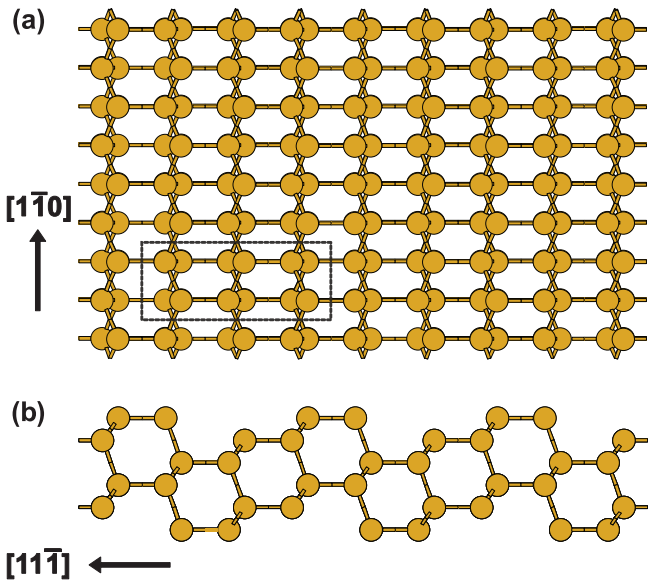

FIG. 9. (a) Top and (b) side view of the bulk-terminated Si(112) surface.

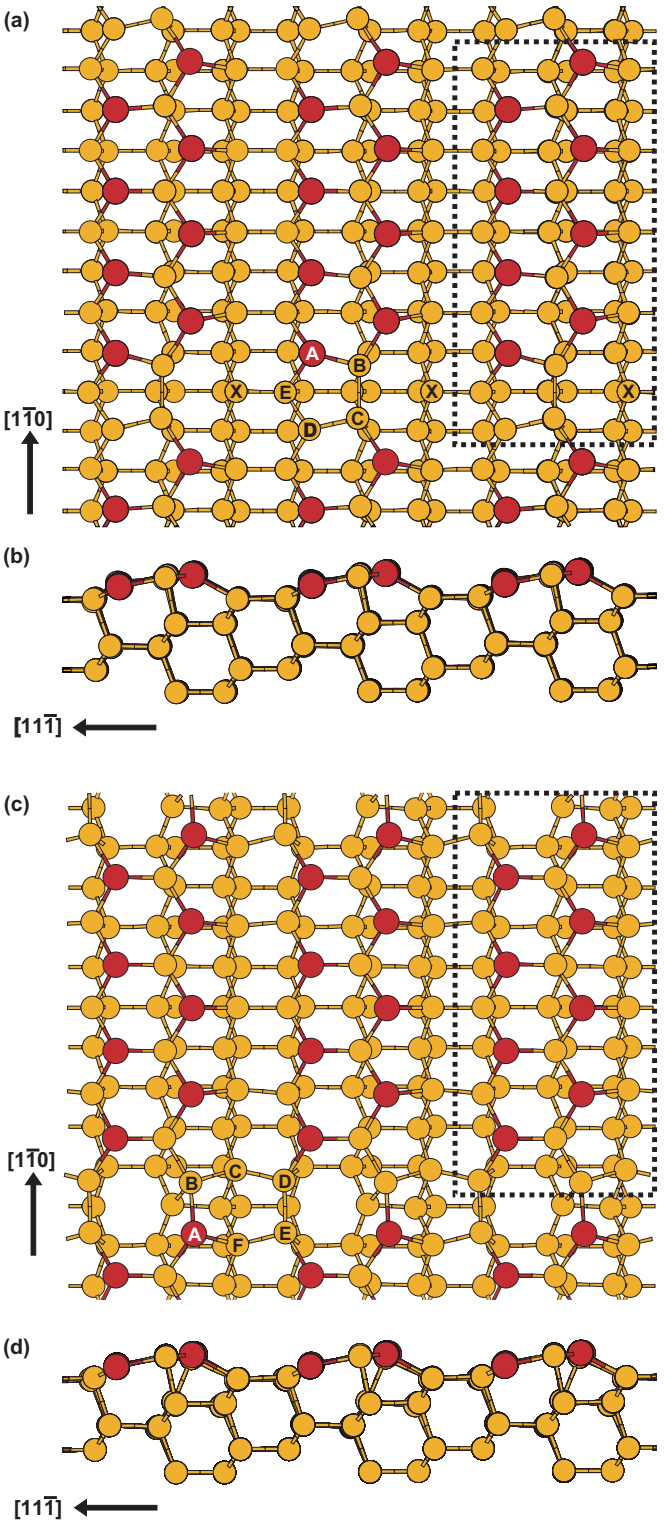

FIG. 10. Top and side view of the Ga/Si(112) structure with two vacancies and a continuous vacancy line (VL). In both cases the model is represented in (5×1) periodicity. In (a) and (b) (Ga-VL-pentamer model), two dangling bonds are found per unit cell (at the positions of the atoms marked with 'D' and 'X', respectively). In (c) and (d) (Ga-VL-hexamer), one Si atom is removed and no dangling bonds are found on the surface. The latter structure is according to the model by Snijders *et al.* [20]. In each top view, one unit cell is indicated. Si atoms are represented in yellow and Ga atoms in red.

TABLE II. Comparison of theoretical (DFT) and experimental (XSW) values of coherent fractions f_c and coherent positions Φ_c, both for the Ga-VL-pentamer (^{p}) [cf. Figs. 10(a) and 10(b)] and for the Ga-VL-hexamer (^{h}) structure [cf. Figs. 10(c) and 10(d)]. The DFT results are shown in (5×1) and (6×1) periodicities. The values for the (5.5×1) structures are averaged from the results for (5×1) and (6×1) periodicity. The last two columns indicate the deviation of the DFT results for these mixed structures from the experimentally determined ones. The bottom row represents mirror-symmetrized (202) and (022) values.

		DFT						XSW	deviation	
reflection	parameter	$(5\times1)^p$	$(6\times1)^p$	$(5.5\times1)^p$	$(5\times1)^h$	$(6\times1)^h$	$(5.5\times1)^h$	$(\overline{N}\times1)$	Δ^p	Δ^h
(111)	f_c	0.75	0.75	0.75	0.75	0.75	0.75	0.71	0.04	0.04
	Φ_c	0.87	0.88	0.87	0.87	0.87	0.87	0.89	0.02	0.02
(113)	f_c	0.57	0.58	0.57	0.63	0.62	0.62	0.38	0.19	0.24
	Φ_c	0.57	0.57	0.57	0.54	0.55	0.54	0.54	0.03	0.00
{202}	f_c	0.62	0.62	0.62	0.56	0.55	0.56	0.38	0.24	0.18
	Φ_c	0.74	0.74	0.74	0.70	0.71	0.70	0.78	0.04	0.08

information about the relaxation of the uppermost Si atoms could be obtained in our XSW experiments, as there was no detectable chemical shift in the Si 1*s* signal.

In order to study the adsorption geometry in more detail, including Si surface relaxations, and to enable a fully three-dimensional structural characterization, i.e., including the Ga and In atomic coordinates along the $[1\bar{1}0]$ direction, complementary DFT calculations on several test configurations have been performed. For reference, the bulk-terminated Si(112) surface is shown in Fig. 9.

From our STM results discussed in Sec. III A and previously presented STM data [19,20], it is obvious that the $(\overline{N}\times1)$ structure of Ga/Si(112) exhibits two Ga vacancies per unit cell, which form a continuous vacancy line (VL). Thus, only those model structures which fulfill these properties were taken into account for the DFT calculations. The atomic arrangement after relaxation by means of our DFT calculations for two possible model structures is depicted for (5×1) periodicity in Figs. 10(a)–10(b) and 10(c)–10(d), respectively, in top and side view.

In both structures, two parallel Ga chains are present in a zigzag configuration, i.e., the atoms in the step-edge chain are shifted by half a (1×1) unit cell size in the $[1\bar{1}0]$ direction compared to atoms in the step-edge chain. Moreover, there are two Ga vacancies, one in each chain. In the first structure, the vacancy in the step-edge chain leads to a Si–Si dimer (B–C), which is part of a mixed pentamer (A–B–C–D–E) with one Ga atom (A) at a step-edge site and two other Si atoms. Therefore, we will refer to this structure as the Ga-VL-pentamer structure in the following. Here, two dangling bonds are found per (5×1) unit cell; one at the atom indicated with 'D' inside the pentamer and a second one at the atom labeled 'X'.

A slightly different situation is present for the structure shown in Figs. 10(c) and 10(d). This is essentially the same model as proposed by Snijders *et al.* [20]. Again, two vacancies are present per unit cell, and each row contains four Ga atoms in case of (5×1) periodicity. But here, one Si atom less is present per unit cell. As a consequence, a Si–Si dimer (D–E) is formed due to the vacancy in the terrace row. The vacancy in the step-edge row forms a Ga–Si dimer (A–B). These two dimers bond to each other via two other Si atoms, leading to the formation of a mixed hexamer (A–B–C–D–E–F) on the surface, consisting of one Ga atom (A) and five Si atoms. Accordingly, we will refer to this structure as a Ga-VL-hexamer structure in the following. For this structure both the tetravalent Si atoms and the trivalent Ga atoms do not have any dangling bonds left and the surface is, thus, fully passivated.

The coherent fractions f_c and coherent positions Φ_c for (111), (113), (202), and (022) Bragg reflections determined from DFT calculations and from XSW measurements are compared in Table II. The DFT results can be found in the six columns indicated with 'DFT,' where the first three (^{p}) belong to the Ga-VL-pentamer structure in Figs. 10(a) and 10(b), and the last three columns (^{h}) belong to the Ga-VL-hexamer structure in Figs. 10(c) and 10(d). Both model configurations were calculated in (5×1) and (6×1) periodicities. In order to compare the results with the experiment (XSW), where an $(\overline{N}\times1)$ periodicity was observed with $\overline{N}$ close to 5.5, the DFT results from configurations with (5×1) and (6×1) periodicity have been averaged to simulate a (5.5×1) structure. Both the Ga-VL-pentamer and the Ga-VL-hexamer structure break the symmetry of the surface, since both models are not mirror symmetric with respect to the $(1\bar{1}0)$ plane. Hence, in the experiment, the surface will consist of two mirror-symmetric domains. The abundance of these two mirror domains should be equal, at least if the influence of other symmetry-breaking features, e.g., step-edges due to miscut, is not too strong. Since the (202) and the (022) directions are transformed into each other under reflection at the $(1\bar{1}0)$ plane, the XSW results in (202) and (022) Bragg reflection should, hence, be identical. Within the experimental uncertainty, this holds at least for the coherent positions, as can be seen from Fig. 6; also for the coherent fractions, there is reasonable agreement. In order to mimic the presence of mirror domains in DFT, the (202) and (022) Fourier components have been averaged. The result is shown in the bottom row of Table II. The deviations Δ^p and Δ^h of the averaged, theoretically determined values from the experimental ones are shown in the last two columns of Table II.

While the rather high deviations for the coherent fractions can be easily explained by a certain experimental disorder on the surface (as mentioned before), the DFT-based values for the coherent positions match quite well with the experimental values. Both models reproduce the experimental values more or less equally and, thus, none of the two models can be preferred solely based on a comparison with the XSW data.

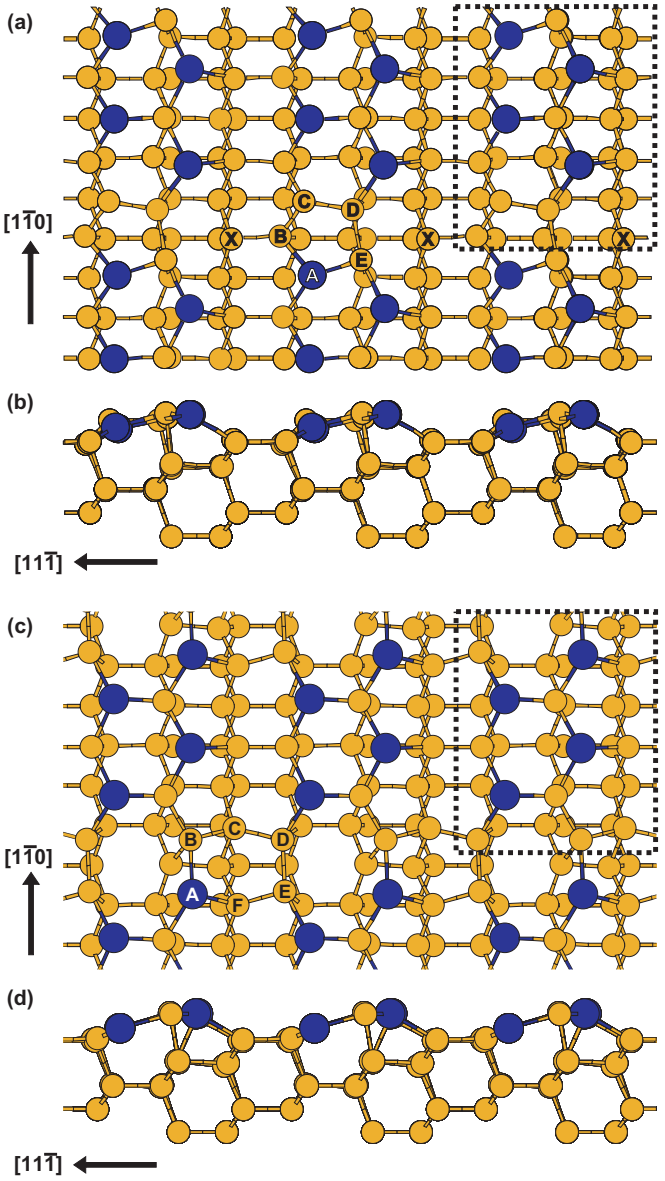

FIG. 11. Top and side view of the In/Si(112) structure in two different models in (3×1) periodicity, determined by DFT calculations. Both models contain two vacancies per unit cell which form a vacancy line (VL). In (a) and (b) (In-VL-pentamer model) two dangling bonds at 'X' and 'C' are found, whereas in (c) and (d) (In-VL-hexamer) no dangling bond is present, analogously to the model by Snijders *et al.* [20] for Ga/Si(112). In each top view, one (3×1) unit cell is indicated. Si atoms are represented in yellow and In atoms in blue. *Note*: These models reproduce the XSW data not as well as the model in Fig. 13.

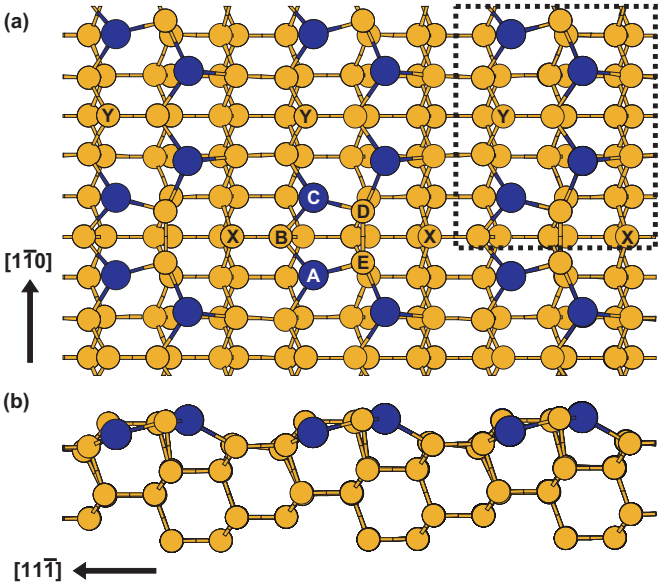

FIG. 12. Top and side view of the In/Si(112) dispersed-vacancy-pentamer structure in (3×1) periodicity, determined by DFT calculations. This model is very similar to the one presented in Figs. 11(a) and 11(b), but the two vacancies ('X' and 'Y') are separated by half a unit cell in [1$\bar{1}$0] direction and, thus, no vacancy line is formed. In the top view one (3×1) unit cell is indicated. Si atoms are represented in yellow and In atoms in blue. *Note*: This model reproduces the XSW data not as well as the model in Fig. 13.

Since the Ga-VL-pentamer structure exhibits two dangling bonds more per unit cell than Ga-VL-hexamer model, it is energetically rather unfavorable. Thus, our DFT results support the Ga-VL-pentamer model as proposed by Snijders *et al.* [20]. Moreover, we were able to substantiate this model with structural, experimental data by means of x-ray standing waves.

To establish a new model for In/Si(112), we tested different model structures and again compared with our XSW data. As first models, the two structures for Ga/Si(112) discussed above were computed in (3×1) and (4×1) periodicities with In instead of Ga. The results of the calculations are depicted in (3×1) periodicity in Figs. 11(a)–11(b) and 11(c)–11(d), respectively. The relaxed configurations resemble those obtained for Ga very much. In both models, a VL is formed. The first structure contains a mixed pentamer as structural element, while in the second, a mixed hexamer can be identified. Therefore, we refer to these structures as In-VL-pentamer and In-VL-hexamer structure in the following. While the In-VL-pentamer structure has two dangling bonds per unit cell (at 'C' and 'X'), the surface is completely saturated in the case of the In-VL-hexamer model.

Another modification of the first structure in Fig. 11 can be found in Fig. 12. Here the two vacancies per unit cell do not form a continuous vacancy line, but they are separated from each other by half a unit cell in the [1$\bar{1}$0] direction. This model is referred to as dispersed-vacancy-pentamer model in the following. Again, two dangling bonds are found per unit cell (at 'X' and 'Y'), but its total energy is around 0.6 eV per unit cell lower than for the structure in Figs. 11(a)–11(b). Interestingly, this structure is the only one discussed so far which maintains the mirror symmetry of the surface. Similar to the single-vacancy-pentamer model to be discussed below, there are (1$\bar{1}$0) mirror planes at the In vacancies.

Although the In/Si(112) structures are very similar to the Ga/Si(112) models, some minor differences are found. In the In-VL-pentamer model in Figs. 11(a)–11(b), a Si-Si dimer (D–E) is induced by the vacancy in the step-edge row. These two Si atoms bond to one In atom (A) and two other Si atoms forming a mixed and slightly *slanted* pentamer (A–B–C–D–E). This is

TABLE III. Comparison of theoretical (DFT) and experimental (XSW) values of coherent fractions f_c and coherent positions Φ_c for different In/Si(112) structures with two vacancies: The In-VL-pentamer model (^{p}) [cf. Figs. 11(a) and 11(b)], the dispersed-vacancy-pentamer model (^{d}) [cf. Fig. 12], and the In-VL-hexamer model (^{h}) [cf. Figs. 11(c) and 11(d)]. The DFT results are shown in (3×1) and (4×1) periodicities. The values for the (3.5×1) structures are averaged from the respective structures with (3×1) and (4×1) periodicity. The last three columns indicate the deviation of the DFT results for these mixed structures from the experimentally determined ones. The bottom row represents mirror-symmetrized values.

		DFT									XSW	deviation		
reflect.	param.	$(3\times1)^p$	$(4\times1)^p$	$(3.5\times1)^p$	$(3\times1)^d$	$(4\times1)^d$	$(3.5\times1)^d$	$(3\times1)^h$	$(4\times1)^h$	$(3.5\times1)^h$	$(\overline{N}\times1)$	Δ^p	Δ^d	Δ^h
(111)	f_c	0.84	0.84	0.84	0.85	0.84	0.84	0.85	0.84	0.84	0.66	0.18	0.18	0.18
	Φ_c	0.86	0.88	0.87	0.86	0.87	0.86	0.85	0.86	0.85	0.90	0.03	0.04	0.05
(113)	f_c	0.73	0.81	0.77	0.70	0.76	0.83	0.86	0.86	0.86	0.45	0.32	0.38	0.41
	Φ_c	0.58	0.61	0.60	0.56	0.60	0.58	0.51	0.57	0.54	0.68	0.08	0.10	0.14
{202}	f_c	0.72	0.71	0.71	0.75	0.74	0.75	0.69	0.56	0.68	0.41	0.30	0.34	0.27
	Φ_c	0.74	0.76	0.75	0.71	0.74	0.73	0.68	0.72	0.69	0.79	0.04	0.06	0.10

in contrast to the Ga-VL-pentamer model in Figs. 10(a)–10(b), where the pentamer is not slanted.

A similar structural element is found for the dispersed-vacancy-pentamer model in Fig. 12. Here, also a Si-Si dimer (D–E) is formed at the step-edge site, which induces the formation of a mixed pentamer (A–B–C–D–E), which is again *not* slanted and includes *two* In atoms (A and C) in this case.

The comparison between the theoretical (DFT) results for the structures depicted in Figs. 11 and 12 and the experimental (XSW) values for the coherent fractions f_c and Φ_c for the In/Si(112) surface are shown in Table III. The first three columns (^{p}) of the DFT results correspond to the In-VL-pentamer structure depicted in Figs. 11(a) and 11(b), the next three columns (^{d}) belong to the dispersed-vacancy-pentamer structure shown in Fig. 12, and the last three DFT columns (^{h}) refer to the In-VL-hexamer structure in Figs. 11(c) and 11(d). Unfortunately, no large differences between the deviations Δ^p, Δ^d, and Δ^h of these three model structures from the experimentally determined values of f_c and Φ_c are found.

A much better agreement of the theoretically determined values with the experimental data is obtained for another structure, including only one vacancy per unit cell in the step-edge row and, thus, a continuous terrace row, as proposed in the model by Gupta and Batra [22] for Al/Si(112)-(6×1). This model again preserves the $(1\bar{1}0)$ mirror symmetry of the Si(112) surface and is referred to as single-vacancy-pentamer model here. The results of the DFT calculations are depicted in Fig. 13 and the comparison of the theoretical with the experimental values of f_c and Φ_c can be found in Table IV. Especially, the coherent positions Φ_c are reproduced nearly perfectly by the DFT results, while the deviations of the DFT-based coherent fractions f_c from the measured ones are in a similar range as those for the structures with two vacancies per unit cell. These deviations can, again, be mostly attributed to experimental uncertainties.

TABLE IV. Comparison between theoretical (DFT) and experimental (XSW) values of coherent fractions f_c and coherent positions Φ_c for the In/Si(112) single-vacancy-pentamer structure, i.e., with one vacancy in the step-edge site (cf. Fig. 13). The DFT results are shown in (3×1) and (4×1) periodicities. Values for the (3.5×1) structure are averaged from the (3×1) and (4×1) structures. The last column indicates the deviation of the DFT results for this mixed structure from the experimentally determined ones. The bottom row represents mirror-symmetrized values.

		DFT			XSW	deviation
reflect.	param.	(3×1)	(4×1)	(3.5×1)	$(\bar{N}\times1)$	Δ
(111)	f_c	0.84	0.83	0.84	0.66	0.18
	Φ_c	0.89	0.90	0.90	0.90	0.00
(113)	f_c	0.78	0.83	0.80	0.45	0.35
	Φ_c	0.64	0.67	0.66	0.68	0.02
{202}	f_c	0.76	0.75	0.76	0.41	0.35
	Φ_c	0.78	0.79	0.78	0.79	0.01

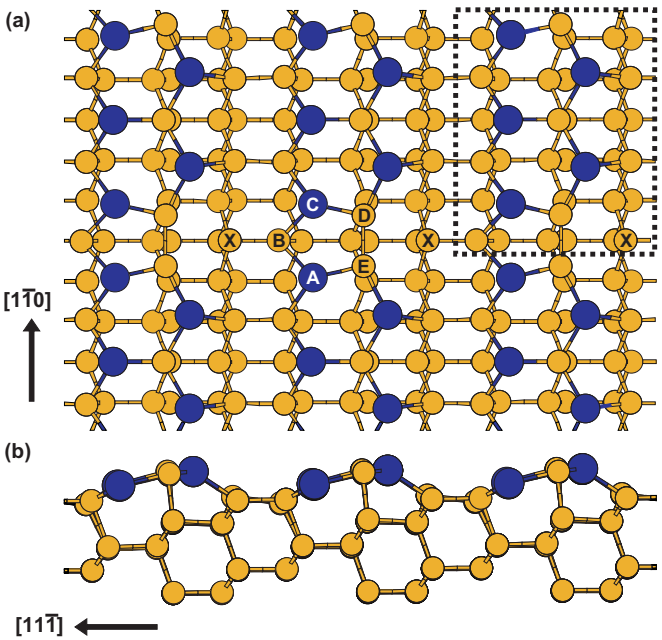

FIG. 13. Top and side view of the In/Si(112) single-vacancy-pentamer structure in (3×1) periodicity, determined by DFT calculations. In this model only one vacancy is found per unit cell (in the step-edge chain) and, thus, a continuous terrace chain is formed. In the top view, one (3×1) unit cell is indicated. Si atoms are represented in yellow and In atoms in blue.

In the model in Fig. 13, five In atoms are found per (3×1) unit cell, three atoms in the terrace row and two in the step-edge row. Due to the vacancy in the step-edge row a Si–Si dimer is formed, which induces the formation of a mixed pentamer (A–B–C–D–E) with another Si atom (B) and two In atoms (A and C) in the terrace site. For this structure the number of dangling bonds is reduced to one per unit cell, which is located at the atom labeled 'X'.

Concluding the discussion on the In/Si(112) structures, the structure with only one vacancy, analogous to the model by Gupta and Batra [22] is clearly favored. It explains both the SPA-LEED data (i.e., a higher saturation coverage than expected for two vacancies) as well as the XSW data and DFT results, since it yields the best agreement with respect to the coherent positions among all candidate structures.

IV. CONCLUSIONS

The adsorption of the group-III metals Ga and In on Si(112) has been analyzed by means of different experimental techniques and complementary DFT calculations. The intrinsically faceted Si(112) surface is found to be smoothed upon adsorption of either of the two metals. In both cases surface structures with a mixture of different $(N\times1)$ unit cells were identified. While at moderate deposition temperature a mixture of mainly (5×1) and (6×1) building blocks are found for Ga adsorption, In adsorption leads to a mixture of (3×1) and (4×1) building blocks. For both Ga/Si(112) and In/Si(112), a temperature dependence and a coverage dependence of the average periodicity $\overline{N}$ is found.

The formation of surface structures including Ga and In vacancies, respectively, have been evidenced by the combination of STM and SPA-LEED results. The internal structure of the $(N\times1)$ building blocks of these structures has been analyzed by means of XSW experiments, the results of which were compared with model structures that were determined using DFT calculations. For Ga/Si(112) and In/Si(112) the $(N\times1)$ building blocks consist of two parallel rows of adsorbate atoms along the $[1\bar{1}0]$ direction, where the atoms of one row occupy terrace (i.e., substitutional) sites, and the atoms of the other row reside on step-edge (i.e., adatom) sites.

The XSW data and DFT calculations for Ga/Si(112) comply with the model by Snijders *et al.* [20] with two vacancies per unit cell (one in the terrace site and one in the step-edge site) and, thus, eight Ga atoms per (5×1) and ten Ga atoms per (6×1) building block, respectively. Although two similar models have equivalently good agreement with the experiment and are, thus, in principle both possible, the Snijders model is energetically more favorable since all dangling bonds are saturated in this model, as suggested by DFT.

For In/Si(112), neither the proposed model for a (7×1)-reconstructed surface by Gai *et al.* [18] (terrace site only) nor the one by Bentmann *et al.* [23] (step-edge site only) could be confirmed. In fact, the best agreement of experiment (XSW) with theory (DFT) is found for a structure where both terrace and step-edge sites are occupied, with one vacancy per unit cell in the step-edge site. This corresponds to five In atoms per (3×1) and seven In atoms per (4×1) building block, respectively. Thus, a new model for the In/Si(112)-$(N\times1)$-structure with only one vacancy per unit cell and a continuous terrace row is proposed, which is analogously configured as the model by Gupta and Batra for the Al/Si(112)-(6×1) structure [22] and which has only one dangling bond per unit cell.

From these findings, the adsorption of group-III metals on Si(112) can be characterized by quite general features. There are common building blocks like one-dimensional atomic chains that are modulated by vacancies, possibly giving rise to specific electronic properties, even charge-density waves. The size of these chains, i.e., the periodicity of the surface reconstruction, can be controlled, to a certain extent, by the metal deposit and by the deposition temperature.

ACKNOWLEDGMENTS

This work has been supported by the Deutsche Forschungsgemeinschaft (Grant No. FA 363/6) and the physics international postgraduate (PIP) programme of the University of Bremen (supported by the German Academic Exchange Service). Parts of the experiments were carried out at the Center for Functional Nanomaterials, BNL, which is supported by the U.S. Department of Energy, Division of Materials Sciences and Division of Chemical Sciences, under Contract No. DE-AC02-98CH10886.

[1] H. Omi and T. Ogino, Appl. Phys. Lett. **71**, 2163 (1997).
[2] A. A. Darhuber, J. Zhu, V. Holý, J. Stangl, P. Mikulík, K. Brunner, G. Abstreiter, and G. Bauer, Appl. Phys. Lett. **73**, 1535 (1998).
[3] K. Brunner, J. Zhu, G. Abstreiter, O. Kienzle, and F. Ernst, Thin Solid Films **369**, 39 (2000).
[4] M. Speckmann, T. Schmidt, A. Locatelli, T. O. Menteş, M. Á. Niño, and J. Falta, Phys. Status Solidi RRL **3**, 305 (2009).
[5] J. K. Dash, A. Rath, R. R. Juluri, P. S. Raman, K. Müller, A. Rosenauer, and P. V. Satyam, J. Phys.: Condens. Matter **23**, 135002 (2011).
[6] L. Du, D. Scopece, G. Springholz, F. Schäffler, and G. Chen, Phys. Rev. B **90**, 075308 (2014).
[7] J. Falta, M. Copel, F. K. LeGoues, and R. M. Tromp, Appl. Phys. Lett. **62**, 2962 (1993).
[8] T. Schmidt, T. Clausen, J. I. Flege, S. Gangopadhyay, A. Locatelli, T. O. Mentes, F. Z. Guo, S. Heun, and J. Falta, New J. Phys. **9**, 392 (2007).
[9] T. Schmidt, J. I. Flege, M. Speckmann, T. Clausen, S. Gangopadhyay, A. Locatelli, T. O. Mentes, S. Heun, F. Z. Guo, P. Sutter, and J. Falta, Phys. Status Solidi A **206**, 1718 (2009).
[10] M. Speckmann, T. Schmidt, J. I. Flege, and J. Falta, IBM J. Res. Dev. **55**, 11 (2011).
[11] Y. Hirose, S. R. Forrest, and A. Kahn, Phys. Rev. B **52**, 14040 (1995).

[12] J. B. Gustafsson, E. Moons, S. M. Widstrand, M. Gurnett, and L. S. O. Johansson, Surf. Sci. **572**, 32 (2004).
[13] C. Ahrens, J. I. Flege, C. Jaye, D. Fischer, T. Schmidt, and J. Falta, J. Phys.: Condens. Matter **28**, 475003 (2016).
[14] A. A. Baski and L. J. Whitman, Phys. Rev. Lett. **74**, 956 (1995).
[15] A. Baski, S. Erwin, and L. Whitman, Surf. Sci. **392**, 69 (1997).
[16] T. M. Jung, S. M. Prokes, and R. Kaplan, J. Vac. Sci. Technol. A **12**, 1838 (1994).
[17] A. A. Baski and L. J. Whitman, J. Vac. Sci. Technol. B **14**, 992 (1996).
[18] Z. Gai, R. G. Zhao, W. S. Yang, and T. Sakurai, Phys. Rev. B **61**, 9928 (2000).
[19] C. González, P. C. Snijders, J. Ortega, R. Pèrez, F. Flores, S. Rogge, and H. H. Weitering, Phys. Rev. Lett. **93**, 126106 (2004).
[20] P. C. Snijders, S. Rogge, C. González, R. Pèrez, J. Ortega, F. Flores, and H. H. Weitering, Phys. Rev. B **72**, 125343 (2005).
[21] O. Moutanabbir, S. Senz, R. Scholz, M. Alexe, Y. Kim, E. Pippel, Y. Wang, C. Wiethoff, T. Nabbefeld, F. Meyer zu Heringdorf, and M. Horn-von Hoegen, ACS Nano **5**, 1313 (2011).
[22] B. C. Gupta and I. P. Batra, Phys. Rev. B **72**, 165352 (2005).
[23] H. Bentmann, J. Houser, and A. A. Demkov, Phys. Rev. B **80**, 085311 (2009).
[24] J. Lander and J. Morrison, Surf. Sci. **2**, 553 (1964).
[25] J. Zegenhagen, M. S. Hybertsen, P. E. Freeland, and J. R. Patel, Phys. Rev. B **38**, 7885 (1988).
[26] R. D. Meade and D. Vanderbilt, Phys. Rev. Lett. **63**, 1404 (1989).
[27] J. R. Patel, J. Zegenhagen, P. E. Freeland, M. S. Hybertsen, J. A. Golovchenko, and D. M. Chen, J. Vac. Sci. Technol. B **7**, 894 (1989).
[28] S. Gangopadhyay, T. Schmidt, and J. Falta, Surf. Sci. **552**, 63 (2004).
[29] A. A. Baski, S. C. Erwin, and L. J. Whitman, Surf. Sci. **423**, L265 (1999).
[30] J. Zegenhagen, J. R. Patel, P. Freeland, D. M. Chen, J. A. Golovchenko, P. Bedrossian, and J. E. Northrup, Phys. Rev. B **39**, 1298 (1989).
[31] J. I. Flege, T. Schmidt, J. Bätjer, M. Çakmak, J. Falta, and G. Materlik, New J. Phys. **7**, 208 (2005).
[32] M. Siebert, T. Schmidt, J. I. Flege, and J. Falta, Phys. Rev. B **72**, 045323 (2005).
[33] J. I. Flege, T. Schmidt, M. Siebert, G. Materlik, and J. Falta, Phys. Rev. B **78**, 085317 (2008).
[34] C. Kumpf, O. Bunk, J. H. Zeysing, Y. Su, M. Nielsen, R. L. Johnson, R. Feidenhans'l, and K. Bechgaard, Phys. Rev. Lett. **85**, 4916 (2000).
[35] C. González, F. Flores, and J. Ortega, Phys. Rev. Lett. **96**, 136101 (2006).
[36] K. Gronwald and M. Henzler, Surf. Sci. **117**, 180 (1982).
[37] M. H. von Hoegen, Z. Kristallogr. **214**, 591 (1999).
[38] J. I. Flege, E. Vescovo, G. Nintzel, L. Lewis, S. Hulbert, and P. Sutter, Nucl. Instrum. Meth. B **261**, 855 (2007).
[39] B. Batterman and H. Cole, Rev. Mod. Phys. **36**, 681 (1964).
[40] J. Zegenhagen, G. Materlik, and W. Uelhoff, J. X-Ray Sci. Technol. **2**, 214 (1990).
[41] S. Baroni, A. D. Corso, S. de Gironcoli, and P. Giannozzi, The PWscf (Plane-Wave Self-Consistent Field) package, http://www.pwscf.org.
[42] P. Giannozzi, S. Baroni, N. Bonini, M. Calandra, R. Car, C. Cavazzoni, D. Ceresoli, G. L. Chiarotti, M. Cococcioni, I. Dabo, A. D. Corso, S. de Gironcoli, S. Fabris, G. Fratesi, R. Gebauer, U. Gerstmann, C. Gougoussis, A. Kokalj, M. Lazzeri, L. Martin-Samos, N. Marzari, F. Mauri, R. Mazzarello, S. Paolini, A. Pasquarello, L. Paulatto, C. Sbraccia, S. Scandolo, G. Sclauzero, A. P. Seitsonen, A. Smogunov, P. Umari, and R. M. Wentzcovitch, J. Phys.: Condens. Matter **21**, 395502 (2009).
[43] G. B. Bachelet, D. R. Hamann, and M. Schlüter, Phys. Rev. B **26**, 4199 (1982).
[44] X. Gonze, R. Stumpf, and M. Scheffler, Phys. Rev. B **44**, 8503 (1991).
[45] P. Zahl, M. Bierkandt, S. Schröder, and A. Klust, Rev. Sci. Instrum. **74**, 1222 (2003).
[46] P. Zahl, T. Wagner, R. Möller, and A. Klust, J. Vac. Sci. Technol. B **28**, C4E39 (2010).
[47] A. A. Baski and L. J. Whitman, J. Vac. Sci. Technol. A **13**, 1469 (1995).
[48] T. Schmidt, S. Gangopadhyay, J. I. Flege, T. Clausen, A. Locatelli, S. Heun, and J. Falta, New J. Phys. **7**, 193 (2005).
[49] H. Hibino and T. Ogino, Phys. Rev. B **54**, 5763 (1996).
[50] J. Nogami, S. I. Park, and C. F. Quate, Phys. Rev. B **36**, 6221 (1987).
[51] J. Kraft, M. G. Ramsey, and F. P. Netzer, Phys. Rev. B **55**, 5384 (1997).
[52] N. Nakamura, K. Anno, and S. Kono, Surf. Sci. **256**, 129 (1991).
[53] J. Wang, H. Wu, R. So, Y. Liu, M. H. Xie, and S. Y. Tong, Phys. Rev. B **72**, 245324 (2005).
[54] A. A. Baski, L. J. Whitman, and S. C. Erwin, Science **269**, 1556 (1995).
[55] M. Speckmann, T. Schmidt, J. I. Flege, J. T. Sadowski, P. Sutter, and J. Falta, J. Phys.: Condens. Matter **21**, 314020 (2009).
[56] S. C. Erwin, A. A. Baski, L. J. Whitman, and R. E. Rudd, Phys. Rev. Lett. **83**, 1818 (1999).
[57] J. Höcker, T. O. Menteş, A. Sala, A. Locatelli, T. Schmidt, J. Falta, S. D. Senanayake, and J. I. Flege, Adv. Mater. Interf. **2**, 1500314 (2015).
[58] J. Zegenhagen, Surf. Sci. Rep. **18**, 202 (1993).
[59] I. A. Vartanyants and J. Zegenhagen, Sol. State Commun. **113**, 299 (1999).
[60] I. A. Vartanyants and J. Zegenhagen, Sol. State Commun. **115**, 161 (2000).
[61] J. Falta, T. Schmidt, A. Hille, and G. Materlik, Phys. Rev. B **54**, R17288 (1996).